Published online 28 July 2007 *Nucleic Acids Research, 2007, Vol. 35, No. 17* ***5913–5921***
doi:10.1093/nar/gkm626

Molecular basis of Diamond–Blackfan anemia: structure and function analysis of RPS19

Lynn A. Gregory[1,2], Almass-Houd Aguissa-Touré[3], Noël Pinaud[1,2], Pierre Legrand[4], Pierre-Emmanuel Gleizes[3,*] and Sébastien Fribourg[1,2,*]

[1]INSERM U869, Institut Européen de Chimie et Biologie, 2 rue Robert Escarpit Pessac, F-33607, [2]Université Victor Segalen, Bordeaux 2, F-33076, [3]Laboratoire de Biologie Moléculaire des eucaryotes (UMR5099) and Institut d'Exploration Fonctionnelle des Génomes (IFR109), CNRS and Université Paul Sabatier, 118 route de Narbonne F-31062 Toulouse and [4]Synchrotron SOLEIL L'Orme des Merisiers, Saint Aubin- BP48, 91192 Gif sur Yvette Cedex, France

Received July 6, 2007; Revised and Accepted July 30, 2007 EBI Accession No. 2v7f

ABSTRACT

Diamond–Blackfan anemia (DBA) is a rare congenital disease linked to mutations in the ribosomal protein genes *rps19*, *rps24* and *rps17*. It belongs to the emerging class of ribosomal disorders. To understand the impact of DBA mutations on RPS19 function, we have solved the crystal structure of RPS19 from *Pyrococcus abyssi*. The protein forms a five α-helix bundle organized around a central amphipathic α-helix, which corresponds to the DBA mutation hot spot. From the structure, we classify DBA mutations relative to their respective impact on protein folding (class I) or on surface properties (class II). Class II mutations cluster into two conserved basic patches. *In vivo* analysis in yeast demonstrates an essential role for class II residues in the incorporation into pre-40S ribosomal particles. This data indicate that missense mutations in DBA primarily affect the capacity of the protein to be incorporated into pre-ribosomes, thus blocking maturation of the pre-40S particles.

INTRODUCTION

Diamond–Blackfan anemia (DBA) is a rare congenital disorder characterized by the defective differentiation of pro-erythroblasts, the precursors of red blood cells. Patients suffer severe anemia and display heterogeneous clinical features including malformations, growth failure and predisposition to cancer (1,2). Linkage analysis has revealed that a quarter of all DBA reported cases are connected to the heterozygous mutation of the gene encoding the ribosomal protein RPS19 (3,4). The RPS19 protein is a component of the 40S ribosomal subunit and belongs to a family of ribosomal proteins restricted to eukaryotes and archea. It is essential for yeast viability and for early stages of development in mice (5,6). Disruption as well as point mutations of the *rps19* gene in yeast and human cells affect maturation of the pre-ribosomal RNA (pre-rRNA) and block production of the 40S ribosomal subunits (5,7–9). Why the mutation of a ribosomal protein primarily affects pro-erythroblast differentiation remains a central question. However, recent linkage of a two other ribosomal protein genes, *rps24* and *rps17*, to DBA (10,11) strongly supports the hypothesis that DBA is the consequence of a ribosomal disorder (8,12).

Over 60 different mutations affecting the *rps19* gene have been reported, including deletions, insertions, frameshifts, premature stop codons and missense mutations (13–15). Some mutations, like very early stop codons or modification of the promoter clearly result in RPS19 haplodeficiency by hampering synthesis of RPS19 from the mutated allele. However, for more subtle mutations like missense mutations, the question arises as to whether they affect the folding of the protein or whether they are milder mutations affecting the function while preserving the overall fold. Since there is no homolog of RPS19 in bacteria, for which high-resolution structures of the small ribosomal subunit are available, the structure of RPS19 and its precise location within the 40S subunit remain unknown. The crystal structure of RPS19 from *Pyroccocus abyssi* presented herein fills this gap and provides a rationale for the impact of RPS19 mutations in DBA.

*To whom correspondence should be addressed. Tel: 00 33 5 40 00 30 63; Fax: 00 33 5 40 00 30 68; Email: s.fribourg@iecb.u-bordeaux.fr
Correspondence may also be addressed to Pierre-Emmanuel Gleizes. Tel/Fax: 00 33 5 61 33 59 26/58 86, Email: gleizes@ibcg.biotoul.fr

The authors wish it to be known that, in their opinion, the first two authors should be regarded as joint First Authors.

MATERIAL AND METHODS

Protein expression, purification and crystallization

Pyrococcus abyssi RPS19 cDNA was cloned into a pET-15b (Novagen) modified plasmid. The expression was carried out in BL21 (DE3) Rosetta cells (Novagen) at 15°C. Bacterial cells were sonicated and centrifuged for 30 min at 50 000 *g*. The supernatant was heated up for 20 min at 50°C and centrifuged for another 30 min at 50 000 *g*. After incubation and elution from the cobalt-affinity resin, the tag was cleaved from the protein by an overnight digest with 1/200 (w/w) ratio with TEV. A step of purification on Hi-S (Pharmacia) was carried out and the protein was eluted at about 600 mM NaCl. The protein was concentrated to up to 10 mg/ml in 50 mM Tris–HCl pH 7.5, 600 mM NaCl. Crystals were obtained at 20°C by the hanging drop vapor diffusion method by mixing equal amounts of the protein solution and of a reservoir composed of 30–36% PEG 2000 MME, 100 mM Tris–HCl pH 6.8–7.5 over a couple days to a size of $50 \times 200 \times 200$ microns. They diffracted to 1.15 Å on synchrotron beamline and belonged to the space group $P2_12_12_1$ with cell dimensions $a = 32$ Å, $b = 57$ Å, $c = 82$ Å and contained one molecule per asymmetric unit and 48% solvent.

Structure solution and refinement

Native and derivative data were collected at the ESRF synchrotron and processed with XDS (16). Data collection statistics are shown in Table 1. A HgBr2 derivative resulting from a 12-h soak in 2.5% (v/v) HgBr2 (prepared from a saturated solution) was collected at the LIII-edge of Hg. Derivative data set was combined with the most isomorphous native data set, SHELXD and SHARP were used to locate and refine the heavy atom site position (17,18). The resulting phases had an overall figure of merit (FOM) of 0.33 at a resolution of 2.0 Å. After solvent flattening with Solomon (SHARP), automatic building was carried out with ARP/wARP (19). Out of a total of 150 residues, 125 were initially placed. Further building and refinement cycles were carried out with Coot and REFMAC (20,21). Last cycles of refinement were carried out including hydrogens and using individual anisotropic B factors.

The final model has a good stereochemistry with an R-free value of 15.5% and a R-factor value of 13.7% (Table 1).

Analysis of RPS19 mutations in yeast

Site-directed mutagenesis on yeast RPS19 was performed by PCR. For complementation experiments, the mutated alleles were subcloned into vector pFL38-Ps15 (URA3), downstream of the constitutive RPS15 promoter. The resulting plasmids were introduced in the *ura3*Δ GAL-RPS19 strain (5). Cells were cultured in liquid synthetic medium containing galactose, but no uracil, and spotted at different densities on agar plates using the same medium, with either galactose or glucose as the carbon source to modulate RPS19 expression.

Table 1. Crystallographic data phasing and refinement statistics

	Native 1	Native 2	Hg derivative
Space group	$P2_12_12_1$	$P2_12_12_1$	$P2_12_12_1$
Cell dimensions			
a, *b*, *c* (Å)	32.70, 57.43, 80.20	31.78, 57.78, 81.03	31.58, 57.39, 81.58
α, β, γ (°)	90.0, 90.0, 90.0	90.0, 90.0, 90.0	90.0, 90.0, 90.0
X-ray source	ID14-4	ID29	ID29
Wavelength (Å)	0.9840	1.0332	1.00932
Resolution (Å)	28–1.15	25–1.9	20–1.91
Total measurements	375 444 (18 387)	75 962 (7898)	78 175 (9427)
Unique reflections	49 876 (5 511)	19 967 (2147)	21 251 (2664)
Redundancy	7.5 (3.3)	3.8 (3.7)	3.7 (3.5)
Completeness (%)	91.5 (72.3)	87.9 (66.0)	94.1 (82.6)
R_{sym} (%)	5.5 (21.2)	6.8 (29.1)	5.6 (15.7)
R_{iso}	23.4 (26.0)[a]		
(Native 2 versus Hg derivative) (%)			
I/σ	22.25 (6.12)	14.01 (4.43)	15.48 (7.64)
FOM (acentric)			0.330
Refinement statistics			
Number of residues	140		
Number of water molecules	186		
Number of ions	2		
RMSD χ^2 bonds (Å)	0.019		
RMSD χ^2 angles (°)	1.818		
R_{work} (%)	13.73		
R_{free} (%)	15.49		

Statistics for high resolution bin (1.15–1.25 Å, 1.9–2.0 Å) are indicated in parentheses.
[a]High resolution bin (2.5–2.6 Å) are indicated in parentheses.

To evaluate incorporation of wild-type or mutated RPS19A into ribosomes, the corresponding open reading frames were also cloned in frame downstream the TAP tag coding sequence in the pFL38-Ps15 vector and expressed in Euroscarf strain Y06271 (*rps19A*::*KanMX*, RPS19B). Whole cell extracts were fractionated by ultracentrifugation on sucrose gradient for ribosome analysis. Two hundred milliliters of yeast culture were grown in YPD medium to an OD_{600} of 0.5 and cycloheximide was added at a final concentration of 100 µg/ml. After 10 min incubation, yeast cells were harvested by centrifugation at 5000 r.p.m and washed in 20 ml ice-cold buffer A [20 mM HEPES (pH 7.5), 10 mM KCl, 5 mM MgCl2, 1 mM EGTA, 1 mM DTT and 100 µg/ml cycloheximide]. Cells were broken with glass beads and re-suspended in 150 µl buffer A. The suspension was clarified by centrifugation for 5 min at 10 000 r.p.m. An amount of the extract corresponding to 1 mg of protein was loaded on a 10.5 ml 10–50% sucrose gradient in buffer A without cycloheximide and centrifuged for 12 h at 26 000 r.p.m in a SW41 rotor. A gradient collector (ÄKTAprime—Amersham Biosciences), in combination with a Pharmacia UV-detector LKB.UV-M II, was used to record the UV profile. Twenty 0.5 ml fractions were collected and 150 µl of each fraction were slot-blotted on nitrocellulose membrane to detect TAP-tagged RPS19A. The membrane was then incubated with

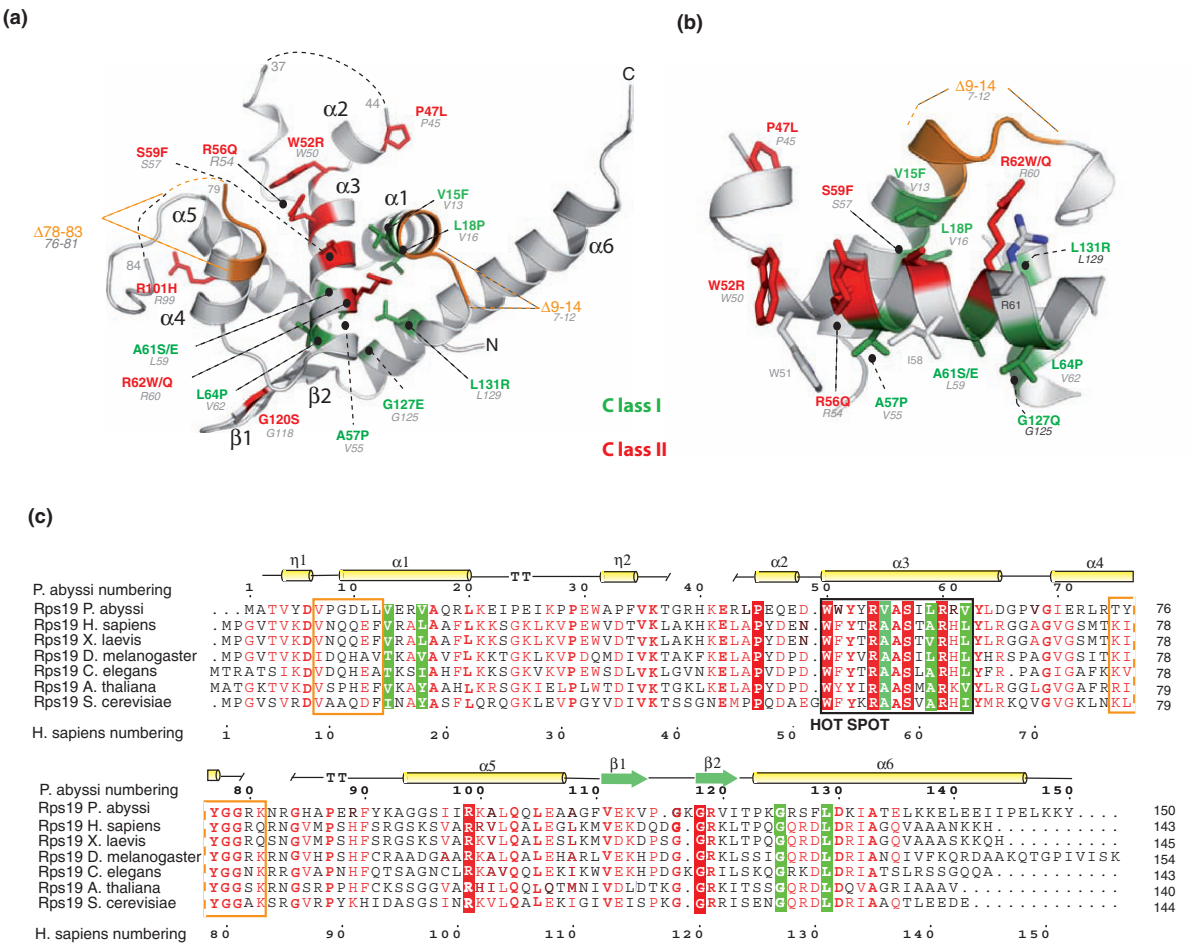

Figure 1. RPS19 structure and sequence alignment. (**a**) Overall structure of RPS19 and point mutations found in DBA patients. Residues labeled in green and red correspond to structural residues (class I) and to solvent accessible residues (class II), respectively. Green and red numbers correspond to human numbering. Gray numbers correspond to *P. abyssi* numbering. Deletions encountered in DBA patients are shown in orange. Dashed lines correspond to disordered loops in the structure. (**b**) The hot spot of mutations. Mutated residues found in and around the hot spot of mutation are shown as in (a). (**c**) Sequence alignment of RPS19 orthologs. RPS19 ortholog sequences have been retrieved and aligned using PipeAlign program suite (31). Class I (boxed in green) and class II (boxed in red) residues are displayed. Deletions encountered in DBA patients are show as orange boxes. Secondary sequence elements are shown on top of the sequence.

peroxidase anti-peroxidase complexes (Sigma), which were revealed by chemoluminescence (ECL, GE Healthcare). After scanning of the film to obtain a digital image, the labeling intensity for each fraction was quantified by densitometry using MetaMorph (Universal Imaging). The UV profiles were superimposed with the blot quantifications to obtain Figure 5.

Ribosomal RNAs were co-immunoprecipitated with RPS19-TAP and analysed as published previously (22,23). Pre-rRNAs were detected on northern blots with probe D-A2 (5′-GAAATCTCTCACCGTTTGGAATAGC-3′) and A2-A3 (5′-ATGAAAACTCCACAGTG-3′).

RESULTS AND DISCUSSION

Overall structure of RPS19

The structure of RPS19 from *P. abyssi* (RPS19^{Pa}) was determined by SIRAS on a mercury derivative and refined against the best native data set. The final model has an R-free value of 15.5% (Table 1) and comprises residues 2 to 150 with the exception of two disordered loops between residues 37–44 and 79–84 (Figure 1a). The structure of RPS19 is almost entirely α-helical and folds around a five α-helix bundle. Knowing that human RPS19 (RPS19^{Hs}) shares 36% identity and 57% similarity with *P. abyssi* RPS19 (RPS19^{Pa}) sequence (Figure 1c), we may assume that they display a similar fold. In the rest of the text, RPS19 residues in *P. abyssi, Saccharomyces cerevisiae* and *Homo sapiens* are labeled 'Pa', 'Sc' and 'Hs' respectively (Table 2).

Two distinct classes of mutations in DBA patients cluster around an amphipathic helix

Fourteen amino acids of RPS19 are the targets of missense mutations in DBA patients. Although these mutations are spread along the entire primary sequence (Figure 1c), the structure of RPS19^{Pa} shows that most missense mutations cluster within or around the α-helix 3 (Figure 1a). This α-helix, made of residues 50–65 of RPS19^{Pa} (52–67 in human numbering), corresponds to the mutation hot spot. It is located at a central position in the

structure where it bridges α-helices 1 and 6 on one side with α-helices 4 and 5 on the other side (Figure 1a). The apolar side of α-helix 3 is engaged into hydrophobic interactions with residues of the neighboring α-helices, thus forming the hydrophobic core of the protein (Figure 1b). Strikingly, three mutations on α-helix 3 (A57P^{Hs}, A61S/E^{Hs}, L64P^{Hs}), two on α-helix 1 (V15F^{Hs} and L18P^{Hs}) and two on α-helix 6 (G127E^{Hs} and L131R^{Hs}) affect residues involved in this hydrophobic core (green residues on Figure 1). Thus, although distant on the primary sequence, these seven amino acids are functionally related and are involved in the folding and the stability of the protein.

In contrast, mutations P47L^{Hs}, W52R^{Hs}, R56Q^{Hs}, S59F^{Hs}, R62W/Q^{Hs}, R101H^{Hs} and G120S^{Hs} affect residues located on the surface of RPS19 (red residues on Figure 1). Remarkably, these residues show a much higher degree of inter-species conservation than the amino acids within the hydrophobic core (Figure 1c). These residues are located within two highly conserved basic patches at the surface of the protein (Figure 2). On the polar face of α-helix 3, four exposed mutated residues (W52^{Hs}, R56^{Hs}, S59^{Hs} and R62^{Hs}) form the floor of a central basic groove (patch A on Figure 2a–c). In addition, residues from α-helices 4 and 5 and from the β-sheet define the conserved patch B (Figure 2d–f). It comprises residues R99^{Pa} (R101^{Hs}), K100^{Pa} (R102^{Hs}), Q103^{Pa} (Q105^{Hs}), K113^{Pa} (K115^{Hs}), G118^{Pa} (G120^{Hs}) and R119^{Pa} (R121^{Hs}). DBA mutations R101H^{Hs} and G120S^{Hs} affect this conserved surface. Interestingly, both conserved surfaces have a positive electrostatic charge: patch A harbors a localized positive charge (Figure 2c), whereas patch B is embedded in a larger positive area (Figure 2f).

Based on these observations, we propose to subdivide DBA mutations into two classes: class I encompasses

Table 2. Amino acid correspondence in Human, yeast and *P. abyssi*

P, abyssi	Yeast	Human	DBA mutation	Class
V13	I15	V15	V15F	I
V16	Y18	L18	L18P	I
P45	P47	P47	P47L	II
W50	W53	W52	W52R	II
R54	R57	R56	R56Q	II
V55	A58	A57	A57P	I
S57	S60	S59	S59F	II
L59	A62	A61	A61S/E	I
R60	R63	R62	R62W/Q	II
V62	I65	L64	L64P	I
R99	R102	R101	R101H	II
G118	G121	G120	G120S	II
R119	R122	R120	-	
G125	G128	G127	G127E	I
S127	R130	R129	-	
L129	L132	L131	L131R	I
K131	R134	R133	-	

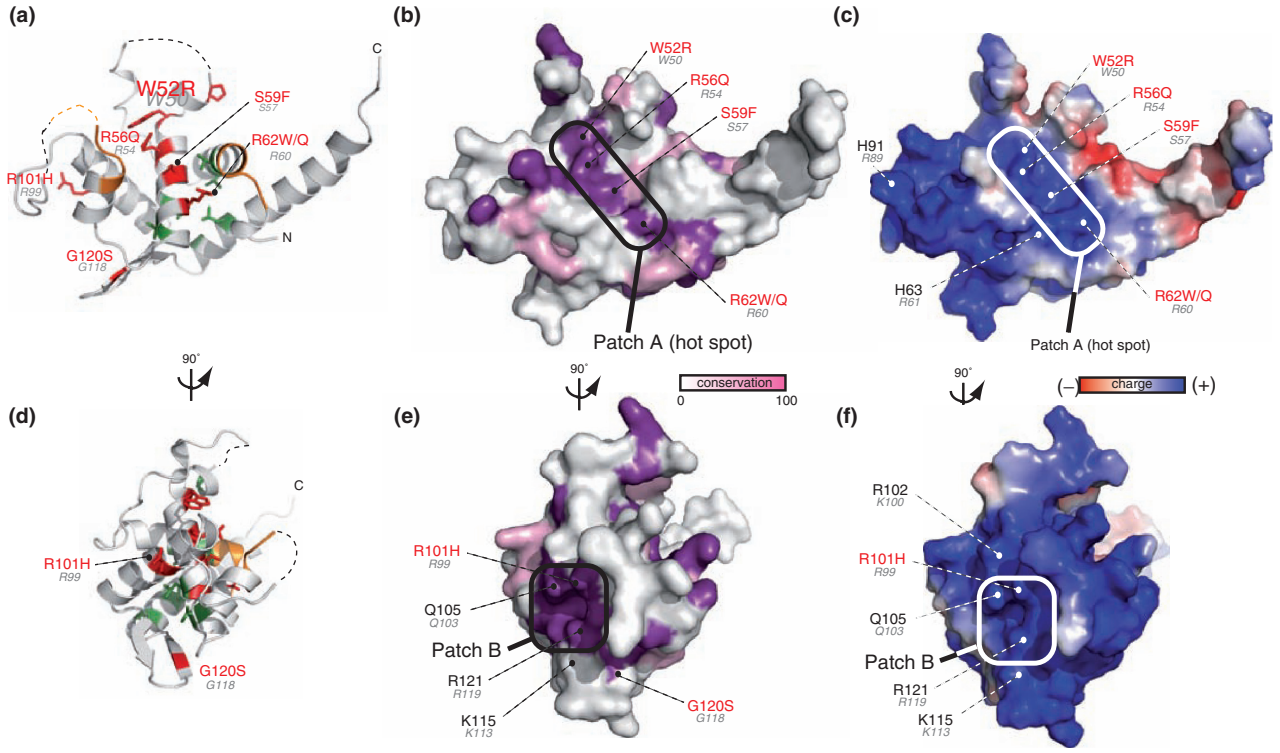

Figure 2. Inter-species conservation and electrostatic surface properties of RPS19. Panels a–c and panels d–f are presented under the same orientation, respectively. (**a**) and (**d**) Ribbon diagrams of RPS19. (**b**) and (**e**) Surface residue conservation of RPS19. Surface conservation was calculated based on the sequence alignment shown in Figure 1 and using ConSurf server with default parameters (32). Conservation is displayed according to white (non-conserved) to purple (100% conservation). Conserved regions are circled in black. Numbering follows the same rule as in Figure 1. (**c**) and (**f**) Electrostatic charge distribution on the surface of RPS19 was calculated using APBS program default parameters (33). Highly conserved and charged areas are boxed.

structural residues affecting the folding of the protein; class II mutations affect surface residues and would impair the function of RPS19 without altering its overall fold. It should be noted that the Val13^{Pa} (V15F^{Hs}) and W50^{Pa} (W52R^{Hs}) are partially involved in Van der Waals contacts with neighboring atoms and are also partially exposed to the solvent. Class I mutations affecting protein folding are predicted to render the protein unstable. Indeed, when expressed in COS cells, mutant RPS19 V15F^{Hs} and G127E^{Hs} were shown to be present at low level, in contrast to class II mutants R56Q^{Hs}, R62W^{Hs} whose level was similar to that of wild-type RPS19 (24,25). Along this line, a recent report confirms and extends these results by showing that class I mutants V15F^{Hs}, L18P^{Hs}, A57P^{Hs}, A61S/E^{Hs}, G127E^{Hs} and L131P^{Hs} are rapidly degraded by the proteasome when expressed in mammalian cells, whereas class II mutants P47L^{Hs}, W52R^{Hs}, R56Q^{Hs}, R62W^{Hs}, R62Q^{Hs}, R101H^{Hs}, are G120S^{Hs} are more stable (26). Thus, the classification proposed here perfectly correlates with the instability observed for class I mutants expressed in cultured cells.

The conserved basic patches are critical for RPS19 function

In order to test whether the conserved surface areas are essential for the function RPS19, we performed functional complementation in yeast. RPS19 is encoded by two genes, *RPS19A* and *RPS19B, in S. cerevisiae*. DBA-like mutations, as well as systematic R to E mutations that alter the charge of these basic conserved areas, were introduced by site-directed mutagenesis into the *RPS19A* gene. The ability of these mutant alleles to support growth was evaluated in a *rps19A*Δ *rps19B*Δ mutant strain conditionally expressing the wild-type RPS19A under control of a galactose promoter. As shown in Figure 3, DBA mutations R57Q^{Sc}, R63Q^{Sc} and R102H^{Sc} had a drastic effect on RPS19 capacity to support cell growth in glucose, whereas mutation R63W^{Sc} partially supported growth. Similarly, mutation to glutamic acid of R57^{Sc}, S60^{Sc} and R63^{Sc} in patch A and R102^{Sc}, R122^{Sc} in patch B, completely abolished cell growth. In contrast, the double mutation R130E-R134E, outside of the conserved patches, had little impact on viability. These results show the crucial role of basic patches A and B in RPS19 function.

As already observed with this assay (23), among class I mutations, I65P^{Sc} (L64P^{Hs}) was not viable, I15F^{Sc} (V15F^{Hs}) strongly affected RPS19 function, whereas substitution A62S^{Sc} (A61S^{Hs}) had little impact on cell growth, which was also the case for class II mutation G121S^{Sc} (G120S^{Hs}). Although affecting highly conserved residues, these two latter mutations may have more critical effects in human than in yeast.

Requirement of patches A and B for RPS19 incorporation into pre-ribosomes

In order to further characterize the loss-of-function associated with mutation of surface residues, we tested whether class II mutations affected RPS19 incorporation into pre-ribosomes. We thus analysed association of RPS19 mutants with pre-ribosomal RNAs in yeast. TAP tagged wild-type and mutant alleles of *RPS19A* were expressed in place of the endogenous *RPS19A* gene in a *rps19A*Δ/*RPS19B*$^{+}$ strain. Production of RPS19 in this strain is insufficient and pre-rRNA processing is partially defective (5), which mimics RPS19 haploinsufficiency in DBA patients. Using the complementation assay described in Figure 3, we checked that the RPS19-TAP protein remained functional (data not shown).

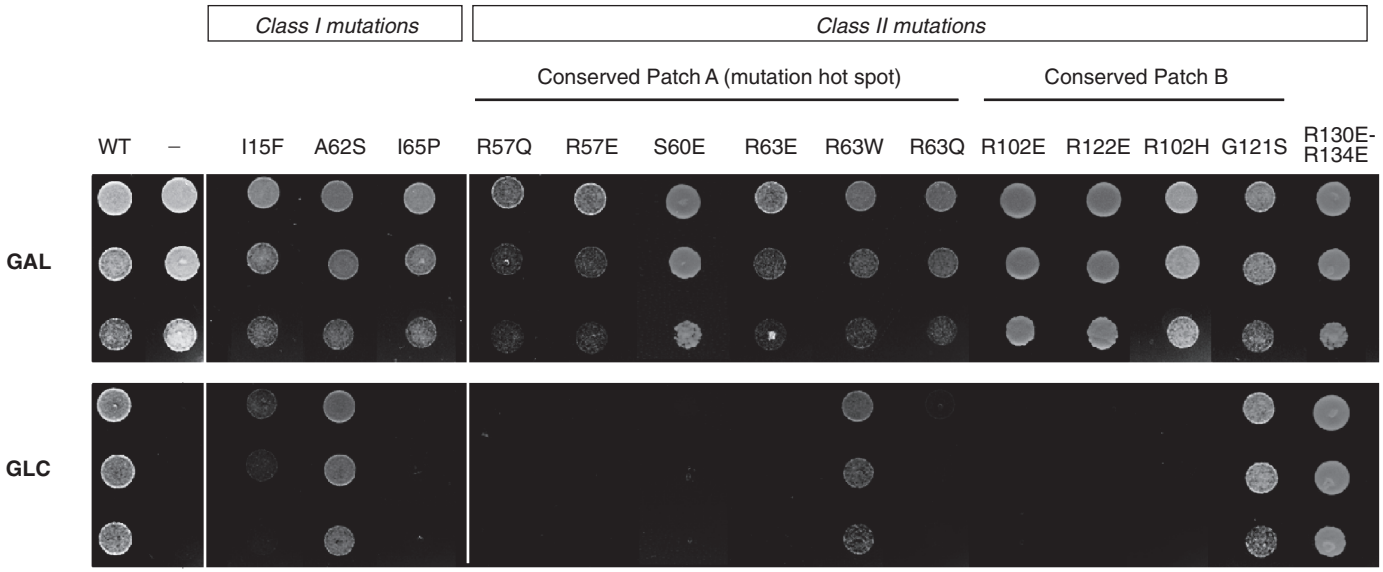

Figure 3. Effect of mutations on RPS19 function in yeast. Capacity of various RPS19 mutants to complement RPS19 expression knockdown was tested in a yeast strain expressing wild-type RPS19 under control of a GAL promoter. Expression of wild-type *RPS19* gene is shutdown upon transfer to glucose containing medium whereas transcription of the mutant forms is driven by a constitutive promoter. Cells were spotted at three different densities.

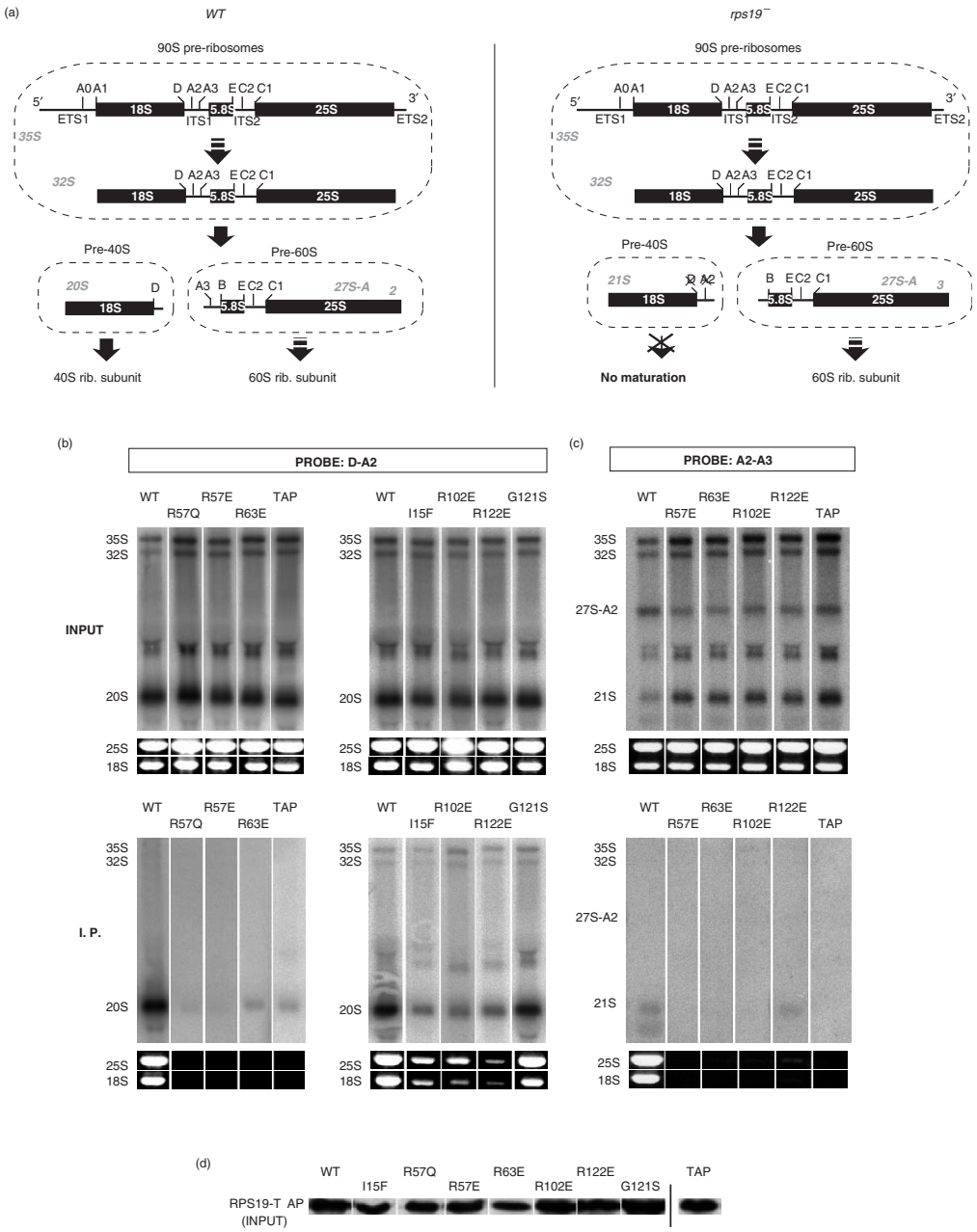

Figure 4. Co-immunoprecipitation of precursor and mature ribosomal RNAs with RPS19-TAP. (**a**) Schematic of pre-rRNA processing in wild-type (top panel) or rps19 deficient cells (lower panel). Letters above pre-rRNAs indicate cleavage sites. (**b, c**) TAP-tagged wild-type or mutated RPS19A expressed in *rps19AΔ*/RPS19B yeast cells were isolated with IgG Sepharose beads. Pre-rRNAs in the whole cell extract ('Input') and the isolated material ('I.P.') were analyzed by northern blot with probes complementary to segment D-A2 (panel B) or to segment A2-A3 (panel C). The mature 18S and 25S rRNAs were detected by ethidium bromide staining. The three panels correspond to independent experiments. In panels A and C, expression of the sole TAP tag was used as a negative control (TAP). The precipitation background level was also evaluated by detecting the 27S-B pre-rRNA with a probe complementary to the ITS2 (data not shown): <0.1% was co-precipitated in panel A and C, <0.3% in panel B, as measured by phosphorimaging. The portion of co-precipitated 20S, 18S and 25S RNAs did not significantly exceed the background value in all panels, except for the wild-type and G121S forms (1–3% of co-precipitation). (**d**) Levels of TAP-tagged proteins in inputs (corresponding to panel A) were analyzed by western blot with peroxidase anti-peroxidase antibody complexes, which bind to protein A.

When captured on IgG Sepharose, the wild-type RPS19-TAP and the G121S^{Sc} mutant co-precipitated with the 18S and 25S rRNAs (Figure 4b, lower panel), indicating incorporation into mature ribosomes (not dissociated under our experimental conditions). Detection of the precursors of the 18S rRNA, by northern blot analysis with the D-A2 probe, showed co-precipitation of the 20S pre-rRNA (Figure 4a, upper panel), the direct precursor to the 18S rRNA (Figure 4b). This indicates the presence of these proteins in pre-40S particles. The 32S and 35S pre-rRNAs, which are part of the early 90S pre-ribosomes, were undetectable or close to

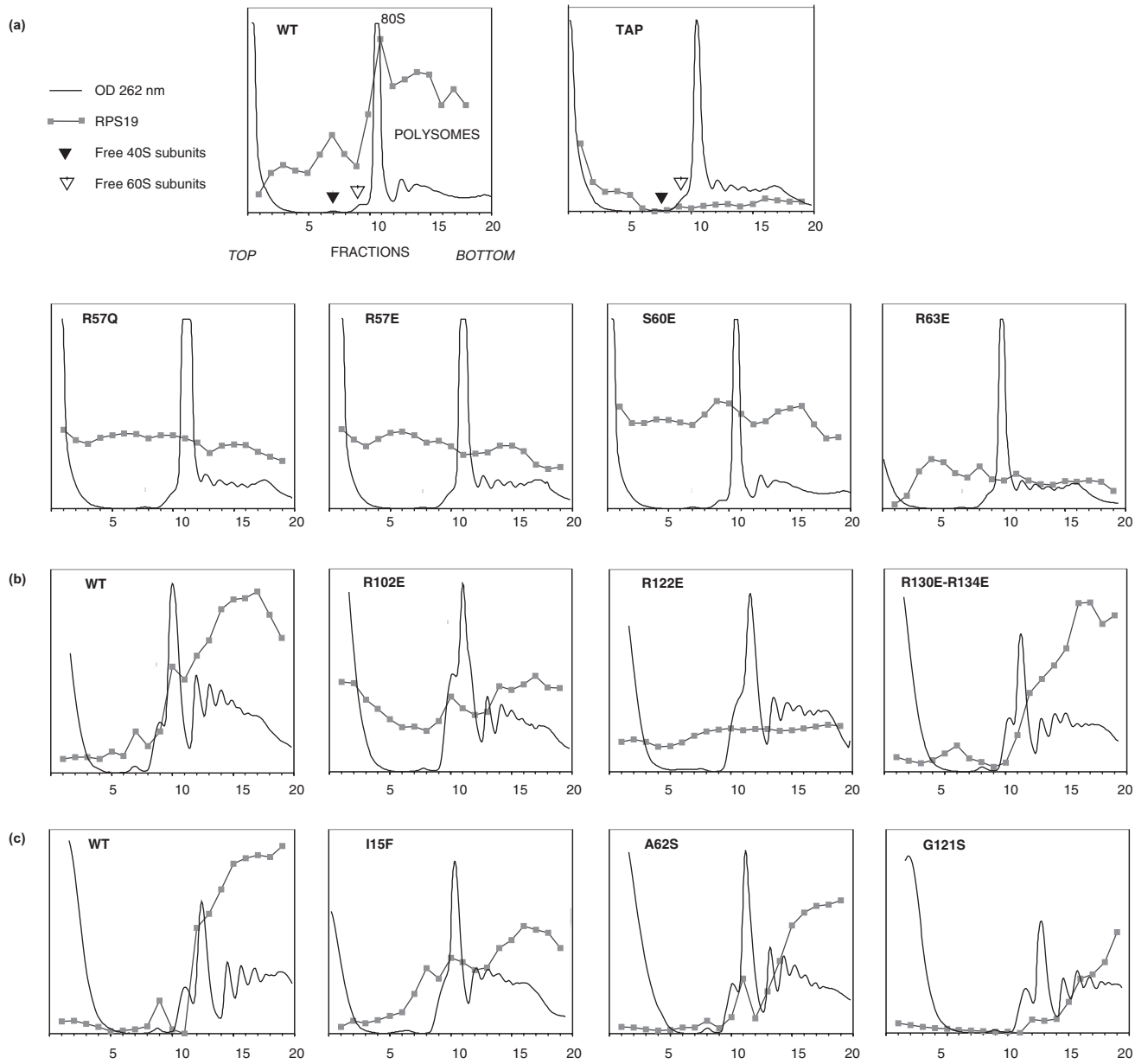

Figure 5. Analysis of wild-type and mutant RPS19 association to ribosomes on sucrose gradient.Ribosomes from *rps19A*Δ/RPS19B yeast strains expressing wild-type or mutated forms of RPS19A fused to the TAP tag were separated on sucrose gradient as described in material and methods. RPS19-TAP was detected in gradient fractions on slot blots with peroxidase. Panels **a, b** and **c** correspond to three series of experiments. Experiments were performed two or three times with similar results. Expression of the sole TAP tag was used as a negative control (TAP).

background in the precipitated fractions, depending on the experiments.

Mutations in basic patch A ($R57E^{Sc}$, $R57Q^{Sc}$, $R63E^{Sc}$) or basic patch B ($R102E^{Sc}$, $R122E^{Sc}$) reduced the amount of co-precipitated mature 18S and 25S rRNAs to background level (Figure 4b and c, lower panel). A similar result was obtained with class I mutation $I15F^{Sc}$. In addition, these proteins did not co-purify with 20S pre-rRNA (Figure 4b). This result was not correlated with differences in protein expression levels of the various mutants (Figure 4d). Cleavage of the 32S pre-rRNA in the early 90S pre-ribosomal particles normally yields the 20S and 27S-A2 pre-rRNAs, included in the pre-40S and pre-60S particles, respectively (Figure 4a, left panel). Deficiency in RPS19 was shown to block cleavage at site A2 (5); alternative cleavage at site A3 produces the 21S and 27S-A3 pre-rRNAs, as illustrated in figure 4a (right panel). We thus considered the hypothesis that RPS19 mutants were incorporated into ill-matured pre-40S particles containing 21S pre-rRNA instead of 20S. As expected, a significant increase in the amount of 21S pre-rRNA, paralleled by a drop in the 27S-A2 pre-rRNA level, was detected in cells expressing RPS19-TAP with mutations $R57E^{Sc}$, $R63E^{Sc}$, $R102E^{Sc}$ or $R122E^{Sc}$

(Figure 4c, 'input'). However, the 21S pre-rRNA did not co-precipitate with mutated RPS19-TAP (Figure 4c, 'I. P.'). Thus, mutation of the basic patches A and B prevents incorporation of RPS19 into pre-ribosomal particles.

These data were fully consistent with the analysis of RPS19 association with ribosomes on sucrose gradients. As shown in Figure 5a, the wild-type TAP-RPS19 protein was mostly present in the fractions containing the 40S subunits, the 80S ribosomes and the polysomes, indicating very efficient incorporation into mature subunits. In contrast, mutations in conserved patches A and B resulted in a large amount of free protein at the top of the gradient, with no preferential association with mature ribosomes (Figure 5a,b). Noticeably, part of these mutated forms of RPS19 was present in high-density fractions. The $A62S^{Sc}$ and $G121S^{Sc}$ mutants, as well as double mutant $R130E^{Sc}/R134E^{Sc}$ (outside of the conserved basic patches), which all support growth in RPS19 depleted yeast, showed an association profile very close to that of wild-type RPS19 (Figure 5c). The $I15F^{Sc}$ mutation, which does not totally abrogate RPS19 function in yeast, showed partial association with mature ribosomes (Figure 5c).

These results indicate that the solvent accessible residues in the mutation hot spot (patch A) or in basic patch B play a critical role in the incorporation of RPS19 into pre-ribosomes. This may involve direct interaction with pre-ribosomal RNA, as supported by the positive charge of these domains, and/or with ribosomal proteins.

In conclusion, we propose that DBA missense mutations primarily result in RPS19 haplodeficiency, by impacting either its folding and its stability, or its capacity to engage intermolecular interactions. The DBA mutation hot spot appears as a key structural element of RPS19 involved both in the constitution of the hydrophobic core and in a highly conserved surface. Impairment of ribosome biogenesis resulting from RPS19 haplodeficiency may have two direct consequences. First, a low rate of small ribosomal subunit production may limit the cell translation capacity (25). Second, alteration of ribosome biogenesis, and subsequently of the nucleolus organization (7), may be perceived by the cell as a 'nucleolar stress' and favor cell cycle arrest (27–29) These phenomena, alone or in combination, could prevent differentiation of pro-erythroblasts (7,12,30). In addition, our data do not exclude a dominant negative effect of the missense mutants, upstream or aside of association with pre-ribosomes, especially in the case of the more stable class II mutants. Presence of some mutants in high-density fractions of the sucrose gradient suggests that they may be engaged in multi-molecular complexes, different from ribosomes, and whose composition remains to be determined. Establishing genotype/phenotype relationships has proved difficult in DBA and this remains true when considering the relative clinical impacts of class I and class II mutations. Availability of RPS19 crystal structure should be decisive to design new strategies to understand RPS19 function and its role in erythropoiesis.

PDB code: PDB coordinates and structure factors have been deposited at the PDB under accession number 2v7f.

ACKNOWLEDGEMENTS

We are grateful to Marlène Faubladier, Guillaume Stahl, Valérie Choesmel and Isabelle Leger-Silvestre for scientific discussion and technical support, to Steven Ellis (Univ. Louisville, USA) for sharing yeast strains, and to the staff members of ID29 and ID14-4 beamlines at ESRF, France. This work was funded by the Agence Nationale pour la Recherche (RIBODBA project) and supported by post-doctoral fellowships from the Conseil Régional d'Aquitaine (L.A.G.) and INSERM (S.F.), and by a CNRS doctoral fellowship (A-H.A-T.). Funding to pay the Open Access publication charges for this article was provided by the Agence Nationale pour la Recherche (RIBODBA project).

Conflict of interest statement. None declared.

REFERENCES

1. Da Costa,L., Willig,T.N., Fixler,J., Mohandas,N. and Tchernia,G. (2001) Diamond-Blackfan anemia. *Curr. Opin. Pediatr.*, **13**, 10–15.
2. Willig,T.N., Gazda,H. and Sieff,C.A. (2000) Diamond-Blackfan anemia. *Curr. Opin. Hematol.*, **7**, 85–94.
3. Gustavsson,P., Garelli,E., Draptchinskaia,N., Ball,S., Willig,T.N., Tentler,D., Dianzani,I., Punnett,H.H., Shafer,F.E. *et al.* (1998) Identification of microdeletions spanning the Diamond-Blackfan anemia locus on 19q13 and evidence for genetic heterogeneity. *Am. J. Hum. Genet.*, **63**, 1388–1395.
4. Draptchinskaia,N., Gustavsson,P., Andersson,B., Pettersson,M., Willig,T.N., Dianzani,I., Ball,S., Tchernia,G., Klar,J. *et al.* (1999) The gene encoding ribosomal protein S19 is mutated in Diamond-Blackfan anaemia. *Nat. Genet.*, **21**, 169–175.
5. Leger-Silvestre,I., Caffrey,J.M., Dawaliby,R., Alvarez-Arias,D.A., Gas,N., Bertolone,S.J., Gleizes,P.E. and Ellis,S.R. (2005) Specific role for yeast homologs of the Diamond Blackfan anemia-associated Rps19 protein in ribosome synthesis. *J. Biol. Chem.*, **280**, 38177–38185.
6. Matsson,H., Davey,E.J., Draptchinskaia,N., Hamaguchi,I., Ooka,A., Leveen,P., Forsberg,E., Karlsson,S. and Dahl,N. (2004) Targeted disruption of the ribosomal protein S19 gene is lethal prior to implantation. *Mol. Cell. Biol.*, **24**, 4032–4037.
7. Choesmel,V., Bacqueville,D., Rouquette,J., Noaillac-Depeyre,J., Fribourg,S., Cretien,A., Leblanc,T., Tchernia,G., Da Costa,L. *et al.* (2007) Impaired ribosome biogenesis in Diamond-Blackfan anemia. *Blood*, **109**, 1275–1283.
8. Flygare,J., Aspesi,A., Bailey,J.C., Miyake,K., Caffrey,J.M., Karlsson,S. and Ellis,S.R. (2007) Human RPS19, the gene mutated in Diamond-Blackfan anemia, encodes a ribosomal protein required for the maturation of 40S ribosomal subunits. *Blood*, **109**, 980–986.
9. Idol,R.A., Robledo,S., Du,H.Y., Crimmins,D.L., Wilson,D.B., Ladenson,J.H., Bessler,M. and Mason,P.J. (2007) Cells depleted for RPS19, a protein associated with Diamond Blackfan anemia, show defects in 18S ribosomal RNA synthesis and small ribosomal subunit production. *Blood Cells Mol. Dis.*, **39**, 35–43.
10. Gazda,H.T., Grabowska,A., Merida-Long,L.B., Latawiec,E., Schneider,H.E., Lipton,J.M., Vlachos,A., Atsidaftos,E., Ball,S.E. *et al.* (2006) Ribosomal protein S24 gene is mutated in Diamond-Blackfan anemia. *Am. J. Hum. Genet.*, **79**, 1110–1118.
11. Cmejla,R., Cmejlova,J., Handrkova,H., Petrak,J. and Pospisilova,D. (2007) Ribosomal protein S17 gene (RPS17) is mutated in Diamond-Blackfan anemia. *Hum. Mutat.* (in press).
12. Ellis,S.R. and Massey,A.T. (2006) Diamond Blackfan anemia: a paradigm for a ribosome-based disease. *Med. Hypotheses*, **66**, 643–648.

13. Campagnoli,M.F., Garelli,E., Quarello,P., Carando,A., Varotto,S., Nobili,B., Longoni,D., Pecile,V., Zecca,M. *et al.* (2004) Molecular basis of Diamond-Blackfan anemia: new findings from the Italian registry and a review of the literature. *Haematologica*, **89**, 480–489.
14. Willig,T.N., Draptchinskaia,N., Dianzani,I., Ball,S., Niemeyer,C., Ramenghi,U., Orfali,K., Gustavsson,P., Garelli,E. *et al.* (1999) Mutations in ribosomal protein S19 gene and Diamond Blackfan anemia: wide variations in phenotypic expression. *Blood*, **94**, 4294–4306.
15. Gazda,H.T. and Sieff,C.A. (2006) Recent insights into the pathogenesis of Diamond-Blackfan anaemia. *Br. J. Haematol.*, **135**, 149–157.
16. Kabsch,W. (1993) Automatic processing of rotation diffraction data from crystals of initially unknown symmetry and cell constants. *J. Appl. Cryst.*, **26**, 795–800.
17. Schneider,T.R. and Sheldrick,G.M. (2002) Substructure solution with SHELXD. *Acta Crystallogr. D Biol. Crystallogr.*, **58**, 1772–1779.
18. De La Fortelle,E. and Bricogne,G. (1997) Maximum-likelihood heavy-atom parameter refinement for multiple isomorphous replacement and multiwavelength anomalous diffraction methods. *Methods Enzymol.*, **472**, 472–494.
19. Cohen,S.X., Morris,R.J., Fernandez,F.J., Ben Jelloul,M., Kakaris,M., Parthasarathy,V., Lamzin,V.S., Kleywegt,G.J. and Perrakis,A. (2004) Towards complete validated models in the next generation of ARP/wARP. *Acta Crystallogr. D Biol. Crystallogr.*, **60**, 2222–2229.
20. Emsley,P. and Cowtan,K. (2004) Coot: model-building tools for molecular graphics. *Acta Crystallogr, D Biol, Crystallogr.*, **60**, 2126–2132.
21. Winn,M.D., Isupov,M.N. and Murshudov,G.N. (2001) Use of TLS parameters to model anisotropic displacements in macromolecular refinement. *Acta Crystallogr. D Biol. Crystallogr.*, **57**, 122–133.
22. Dez,C., Noaillac-Depeyre,J., Caizergues-Ferrer,M. and Henry,Y. (2002) Naf1p, an essential nucleoplasmic factor specifically required for accumulation of box H/ACA small nucleolar RNPs. *Mol. Cell. Biol.*, **22**, 7053–7065.
23. Leger-Silvestre,I., Milkereit,P., Ferreira-Cerca,S., Saveanu,C., Rousselle,J.C., Choesmel,V., Guinefoleau,C., Gas,N. and Gleizes,P.E. (2004) The ribosomal protein Rps15p is required for nuclear exit of the 40S subunit precursors in yeast. *EMBO J.*, **23**, 2336–2347.
24. Da Costa,L., Tchernia,G., Gascard,P., Lo,A., Meerpohl,J., Niemeyer,C., Chasis,J.A., Fixler,J. and Mohandas,N. (2003) Nucleolar localization of RPS19 protein in normal cells and mislocalization due to mutations in the nucleolar localization signals in 2 Diamond-Blackfan anemia patients: potential insights into pathophysiology. *Blood*, **101**, 5039–5045.
25. Cmejlova,J., Dolezalova,L., Pospisilova,D., Petrtylova,K., Petrak,J. and Cmejla,R. (2006) Translational efficiency in patients with Diamond-Blackfan anemia. *Haematologica*, **91**, 1456–1464.
26. Angelini,M., Cannata,S., Mercaldo,V., Gibello,L., Santoro,C., Dianzani,I. and Loreni,F. (2007) Missense mutations associated to Diamond-Blackfan Anemia affect the assembly of ribosomal protein S19 into the ribosome. *Hum. Mol. Genet.*, **16**, 1720–1727.
27. Olson,M.O. (2004) Sensing cellular stress: another new function for the nucleolus? *Sci STKE*, 2004, pe10.
28. Pestov,D.G., Strezoska,Z. and Lau,L.F. (2001) Evidence of p53-dependent cross-talk between ribosome biogenesis and the cell cycle: effects of nucleolar protein Bop1 on G(1)/S transition. *Mol. Cell. Biol.*, **21**, 4246–4255.
29. Rubbi,C.P. and Milner,J. (2003) p53 is a chromatin accessibility factor for nucleotide excision repair of DNA damage. *EMBO J.*, **22**, 975–986.
30. Flygare,J. and Karlsson,S. (2007) Diamond-Blackfan anemia: erythropoiesis lost in translation. *Blood*, **109**, 3152–3154.
31. Plewniak,F., Bianchetti,L., Brelivet,Y., Carles,A., Chalmel,F., Lecompte,O., Mochel,T., Moulinier,L., Muller,A. *et al.* (2003) PipeAlign: a new toolkit for protein family analysis. *Nucleic Acids Res.*, **31**, 3829–3832.
32. Landau,M., Mayrose,I., Rosenberg,Y., Glaser,F., Martz,E., Pupko,T. and Ben-Tal,N. (2005) ConSurf 2005: the projection of evolutionary conservation scores of residues on protein structures. *Nucleic Acids Res.*, **33**, W299–W302.
33. Baker,N.A., Sept,D., Joseph,S., Holst,M.J. and McCammon,J.A. (2001) Electrostatics of nanosystems: application to microtubules and the ribosome. *Proc Natl Acad. Sci. USA*, **98**, 10037–10041.